Supporting Information

Srivastava et al. 10.1073/pnas.1308270110

SI Materials and Methods

Chromatin Immunoprecipitation Sequencing Analysis. Chromatin immunoprecipitation (ChIP) was performed as previously described (1). Specifically, protein–nucleic acid complexes containing CarD hemagglutinin (CarD-HA) were immunoprecipitated from the *Mycobacterium smegmatis* Mc^2155 Δ*carD attB*::tet*carD*-HA strain and unfused HA was immunoprecipitated from the Mc^2155 *attB*::pmsg431 strain (both previously described) (1) with monoclonal antibodies specific for HA (Sigma). RNA polymerase (RNAP) β and σ were immunoprecipitated from Δ*carD attB*::tet*carD*-HA with monoclonal antibodies specific for these subunits (Neoclone; 8RB13 for β, 2G10 for σ). Coprecipitated DNA was sequenced using a SOLiD sequencer (Life Technologies), which provided sufficient reads for 100-fold coverage of the genome. The number of sequence reads per base pair was normalized to the total number of reads and expressed as a $\log_2$ value. The reads per base pair from the HA-alone sample served as the background and were subtracted from the other datasets. The sequences of the 16S, 23S, and 5S rRNA are identical in *rrnA* and *rrnB* so the total number of reads for that sequence was split equally between the operons.

The normalized, background-corrected $\log_2$ reads per base pair were then smoothed over a 20-bp window and σ^A and CarD peaks were identified as described previously (2, 3). Briefly, maxima and minima were assigned relative to values ±10 bp. Maxima within 20 bp were merged with the peak location assigned to the maximum with the highest absolute signal value. Adjacent minima were merged analogously. To assess the statistical significance, peaks were divided into 0.1 interval bins with a lower cutoff of peak height of 0.4 $\log_2$ reads per base pair. Starting with the lowest bin, we then calculated the distance of each peak to the nearest gene start and compared these distances to those computed using genome coordinates arbitrarily rotated 1×10^6 bp around the *M. smegmatis* genome. Using the Wilcoxon–Mann–Whitney rank-sum test for nonsimilarity of distributions, σ^A peaks in the 1.1–1.2 peak-height bins and CarD peaks in the 0.5–0.6 peak-height bins were statistically significant (*P* values for similarity of the distributions <0.0001). We then identified σ^A peaks associated with each gene as the closest σ peak upstream from the gene start and CarD peaks associated with the σ^A peaks as the closest CarD peak to each selected σ^A peak.

To calculate average ChIP signals for the aggregate profiles (Fig. 1*A*), we selected a subset of 62 genes meeting the following criteria: (*i*) ≥300 bp in gene length, (*ii*) average RNAP $\log_2$ ChIP signal ≥1.6/bp, (*iii*) associated with a σ^A peak with $\log_2$ ChIP signal ≥3/bp, (*iv*) absence of other σ^A peaks within 500 bp upstream or 1,000 bp downstream of the associated σ^A peak, (*v*) absence of an oppositely oriented gene with an average RNAP $\log_2$ ChIP signal ≥1 upstream from the gene (because an oppositely oriented gene could create a divergent promoter region with potential for overlapping σ^A and CarD ChIP signals), and (*vi*) absence of an upstream gene with average RNAP $\log_2$ ChIP signal >0 within 100 bp upstream from the gene (because such an arrangement would indicate the gene is an internal member of an operon). The RNAP, CarD, and σ^A signals from the 62 genes were then averaged using the distance from the center of the associated σ^A peaks to align the genes.

Expression, Purification, and Crystallization of *Thermus thermophilus* CarD. The gene encoding *Thermus thermophilus* CarD was amplified from *T. thermophilus* HB8 genomic DNA, cloned into the overexpression vector pET SUMO (Invitrogen), and transformed into BL21(DE3) (Novagen). Transformed cells were grown to an $OD_{\lambda 600}$ of ∼0.6 in the presence of 50 μg/mL kanamycin at 37 °C. Expression was then induced with 1 mM isopropyl β-D-thiogalactopyranoside (IPTG) for 4 h at 28 °C. Cells were harvested by centrifugation and resuspended in lysis buffer [20 mM Tris, pH 8.0, 500 mM NaCl, 10% (vol/vol) glycerol, 0.5 mM β-mercaptoethanol (BME) supplemented with 1 mM PMSF and EDTA-free protease-inhibitor mixture (Sigma)] + 10 mM imidazole. Cells were lysed using a continuous-flow French press (Avestin) and the clarified lysate was loaded onto a Ni^{2+}-chelating HiTrap IMAC column (GE Healthcare) and eluted with lysis buffer + 250 mM imidazole. After overnight digestion of the SUMO His-tag using His-tagged ULP-1 protease (Invitrogen), the cleaved sample was dialyzed overnight into lysis buffer + 10 mM imidazole and a second subtractive Ni^{2+}-chelating chromatographic step was used to remove uncleaved protein, His-tagged Ulp-1, and the cleaved His-SUMO tag. The flow through was concentrated and the sample was further purified by size-exclusion chromatography (SD75 column; Amersham Biosciences) in buffer composed of 20 mM Tris, pH 8.0, 0.5 M NaCl, 5% (vol/vol) glycerol, 2 mM DTT, and 1 mM EDTA. The sample was concentrated to 9 mg/mL and buffer exchanged into 20 mM Tris, pH 8.0, 0.1 M NaCl, and 2 mM DTT. For overproduction of selenomethionyl-substituted protein, protein was overexpressed and labeled as previously described (4) and then purified using the same protocol as described above.

X-Ray Structure Determination of CarD. CarD crystals were grown at 22 °C, using hanging-drop vapor diffusion against a crystallization solution of 100 mM Bis-Tris, pH 6.5, 6% (vol/vol) ethylene glycol, and 30% (vol/vol) 1,3 butanediol with a protein concentration of 9 mg/mL and a 1:1 protein:crystallant ratio. Crystals were cryoprotected by rapid transfer into 100 mM Bis-Tris, pH 6.5, 10% (vol/vol) ethylene glycol, and 20% (vol/vol) glycerol. Data were collected at the National Synchrotron Light Source beamline X25. The data were processed using HKL2000 (5), selenomethionyl sites were located using SHELX (6), and single-wavelength anomalous diffraction phases were calculated using SHARP, with density modification using SOLOMON (7). The selenomethionyl-substituted protein crystals were thicker and diffracted to higher resolution (2.4 Å, Table S2) so these data were also used for the final refinement (Table S2). COOT (8) was used for model building and structures were refined using Phenix (9), leading to the final model refined to 2.4 Å with R_{work}/R_{free} of 0.2003/0.2297 (Table S2) and Ramachandran statistics as follows: 96.77% of residues in preferred regions, 3.23% in allowed regions, 0% in disallowed regions. The final model includes two copies of *T. thermophilus* CarD due to noncrystallographic symmetry. Molecule A is modeled from residue 3 to the C-terminal residue 164; an N-terminal S residue (protease cleavage scar from the Ulp-1 cleavage) plus residues 1 and 2 of the native *T. thermophilus* CarD sequence lack electron density and are presumed disordered. Molecule B is modeled from residues 1–164 (only the N-terminal cleavage scar is disordered).

β-Galactosidase Assays. To perform β-galactosidase (βgal) assays during CarD depletion, an *M. smegmatis* strain expressing $CarD^{wt}$ from the *attB* site (mgm1849) (10) or WT *M. smegmatis* Mc^2155 containing the empty pDB19 vector at the *attB* site (control strain) was transformed with pTE-2MOX (expresses WT TetR) (1) and the plasmid pCLS15-AP123-*lacZ* (low-copy KanR episomal plasmid that expresses *lacZ* from the *M. smegmatis rrnA*

promoters in tandem as present in the genome). CarD was depleted as previously described and depletion was confirmed by Western blot (10). *M. smegmatis* Δ*carD attB*::tet*carD*^{WT}, Δ*carD attB*::tet*carD*^{R25E}, Δ*carD attB*::tet*carD*^{R47E}, and Δ*carD attB*::tet*carD*^{W85A} strains (engineered as described in ref. 1) were transformed with pHMG147-AP123-*lacZ* (HygR episomal plasmid that expresses *lacZ* from the *M. smegmatis rrnA* promoters) to perform βgal assays in strains expressing CarD mutants. βgal activity was measured from log-phase cultures by pelleting the cells and washing them three times in Z buffer (60 mM Na_2HPO_4, 60 mM NaH_2PO_4, 10 mM KCl, 1 mM $MgSO_4$, pH 7) before resuspending them in 200 μL of Z buffer and bead beating four times (FastPrep; Thermo Scientific) to lyse the cells. Total protein content in each lysate was measured by BCA assay (Pearce). A 50-mM final concentration of BME was added to the remaining lysate preparation and βgal activity was measured by adding a final concentration of 2 mg/mL ortho-nitrophenyl-β-galactoside (ONPG) solution in Z buffer. Change in $OD_{\lambda 420}$ absorbance was measured over time, using the Epoch Microplate Spectrophotometer (BioTek). βgal activity was calculated using the equation βgal activity = V_{max}/(total protein concentration × volume of lysate) with V_{max} being the rate of change in $OD_{\lambda 420}$ absorbance (measured as the slope).

In Vitro Transcription Assays. CarD proteins used in in vitro transcription assays were diluted into 1× protein storage buffer (10 mM Tris·HCl, pH 8.0, 0.15 M sodium glutamate, 15% (vol/vol) glycerol, 1 mM DTT). CarD (*T. thermophilus* or *Mycobacterium tuberculosis*; 500 nM) was preincubated with its cognate core RNAP (*T. thermophilus* or *Mycobacterium bovis*; 50 nM) for 10 min on ice, followed by the addition of σ^A (*T. thermophilus* or *M. tuberculosis*; 100 nM). After 10 min, linear promoter DNA (50 nM) was added and the reaction brought to 20 μL by dilution with 1× transcription buffer (40 mM Tris-acetate, pH 7.9, 10 mM $MgCl_2$, 1 mM EDTA, 50 μg/mL BSA, 100 mM NaCl, and 1 mM DTT). Reactions were incubated for 10 min at 65 °C (for *T. thermophilus*) or 37 °C (for *M. bovis*) to form open promoter complexes. Transcription was then initiated by the addition of NTPs [200 μM GTP, CTP, and UTP; 50 μM ATP; and 0.1 μL [α-^{32}P]ATP] and competitor DNA (double-stranded FullCon promoter DNA fragment; 1 μM) (11). After 10 min, the reactions were stopped with 2× formamide buffer [98% (vol/vol) formamide, 5 mM EDTA] and run on a 10–12% urea PAGE gel. Products were visualized by phosphorimagery and quantified using ImageJ (12). Promoter fragments were prepared by PCR, electrophoresed on a 2% agarose gel, and gel purified (Qiagen).

Promoter Binding Assays. Reactions were prepared as for the in vitro transcription assays. Briefly, core RNAP (100 nM) was incubated with CarD for 10 min before the addition of σ^A (500 nM). Labeled linear promoter DNA (25 nM) was added and the reactions were incubated at 65 °C (*T. thermophilus*) or 37 °C (*M. bovis*) for 10 min to form open complexes. Once open complexes were formed, they were challenged with competitor DNA (double-stranded FullCon promoter DNA fragment; 1 μM) and a 10-μL aliquot was removed and bound to prewashed filters (MF-membrane filters; Millipore) and immediately washed with 4 mL wash buffer (10 mM Tris·HCl, pH 8.0, 200 mM NaCl). Radioactive signal, corresponding to labeled promoter DNA fragment bound to RNAP, was quantified by phosphorimagery and analyzed using ImageJ (12).

Native Gel Electrophoresis Mobility Shift Assays. A DNA fragment containing the *rrnA* promoter and leader sequences, called *rrnA*PL and corresponding to *M. smegmatis* Mc^{2}155 nucleotides 5029577–5029909, was gel-purified with a QIAquick column (Qiagen). The DNA (250 ng) was labeled with T4 polynucleotide kinase and [γ-^{32}P]ATP. Unincorporated [γ-^{32}P]ATP was removed using a G-50 microcolumn (GE Healthcare). Labeled probe DNA (2×10^4 cpm, ~0.6 ng), 1 μg of LightShift Poly(di/dc) competitor DNA (Thermo Scientific), 10 μg BSA, 200 pmol full-length *M. smegmatis* CarD, the CarD RNA polymerase-interacting domain (CarD-RID) (amino acids 1–67), or the CarD C-terminal domain (CarD-CTD) (amino acids 68–162) were mixed with binding buffer (20 mM Tris, pH 8, 150 mM NaCl) in a total volume of 12 μL and incubated for 20 min at room temperature. Samples were then electrophoresed on 4–20% nondenaturing TBE polyacrylamide gels (Invitrogen), and the gels were dried and exposed to film for detection by autoradiography.

qRT-PCR. RNA was prepared from 5–10 mL of log-phase *M. smegmatis* Δ*carD attB*::tet*carD*^{wt}, Δ*carD attB*::tet*carD*^{R25E}, Δ*carD attB*::tet*carD*^{R47E}, and Δ*carD attB*::tet*carD*^{W85A} cultures and 16S rRNA levels were measured and normalized to *sigA* transcript levels as previously described (1).

Coimmunoprecipitation. Cell lysates were prepared from 50 mL of log-phase *M. smegmatis* Δ*carD attB*::tet*carD*^{WT}-*HA*, Δ*carD attB*::tet*carD*^{R25E}-*HA*, Δ*carD attB*::tet*carD*^{R47E}-*HA*, and Δ*carD attB*::tet*carD*^{W85A}-*HA* (engineered as described in ref. 1) cultures. HA-tagged CarD proteins were immunoprecipitated from each lysate as previously described (10). For the Western blot analyses, CarD-HA and RNAP β were detected using mouse monoclonal antibodies specific for CarD (10) and RNAP β (clone 8RB13; Neoclone), respectively, and goat anti-mouse secondary antibodies conjugated to IRDye 800CW (LI-COR). The amount of signal was measured for fluorescent intensity, using the LI-COR Odyssey Scanner.

1. Stallings CL, et al. (2009) CarD is an essential regulator of rRNA transcription required for Mycobacterium tuberculosis persistence. *Cell* 138(1):146–159.
2. Mooney RA, et al. (2009) Regulator trafficking on bacterial transcription units in vivo. *Mol Cell* 33(1):97–108.
3. Reppas NB, Wade JT, Church GM, Struhl K (2006) The transition between transcriptional initiation and elongation in E. coli is highly variable and often rate limiting. *Mol Cell* 24(5):747–757.
4. Doublié S (1997) Preparation of selenomethionyl proteins for phase determination. *Methods Enzymol* 276:523–530.
5. Otwinowski Z, Minor W (1997) Processing of X-ray diffraction data. *Methods Enzymol* 276:307–326.
6. Sheldrick GM (2008) A short history of SHELX. *Acta Crystallogr A* 64(Pt 1): 112–122.
7. de la Fortelle E, Bricogne G (1997) Maximum-likelihood heavy-atom parameter refinement for multiple isomorphous replacement and multiwavelength anomalous diffraction methods. *Methods Enzymol* 276:472–494.
8. Emsley P, Cowtan K (2004) Coot: Model-building tools for molecular graphics. *Acta Crystallogr D Biol Crystallogr* 60(Pt 12 Pt 1):2126–2132.
9. Adams PD, et al. (2010) PHENIX: A comprehensive Python-based system for macromolecular structure solution. *Acta Crystallogr D Biol Crystallogr* 66(Pt 2):213–221.
10. Weiss LA, et al. (2012) Interaction of CarD with RNA polymerase mediates Mycobacterium tuberculosis viability, rifampin resistance, and pathogenesis. *J Bacteriol* 194(20):5621–5631.
11. Gaal T, et al. (2001) Promoter recognition and discrimination by EsigmaS RNA polymerase. *Mol Microbiol* 42(4):939–954.
12. Schneider CA, Rasband WS, Eliceiri KW (2012) NIH Image to ImageJ: 25 years of image analysis. *Nat Methods* 9(7):671–675.

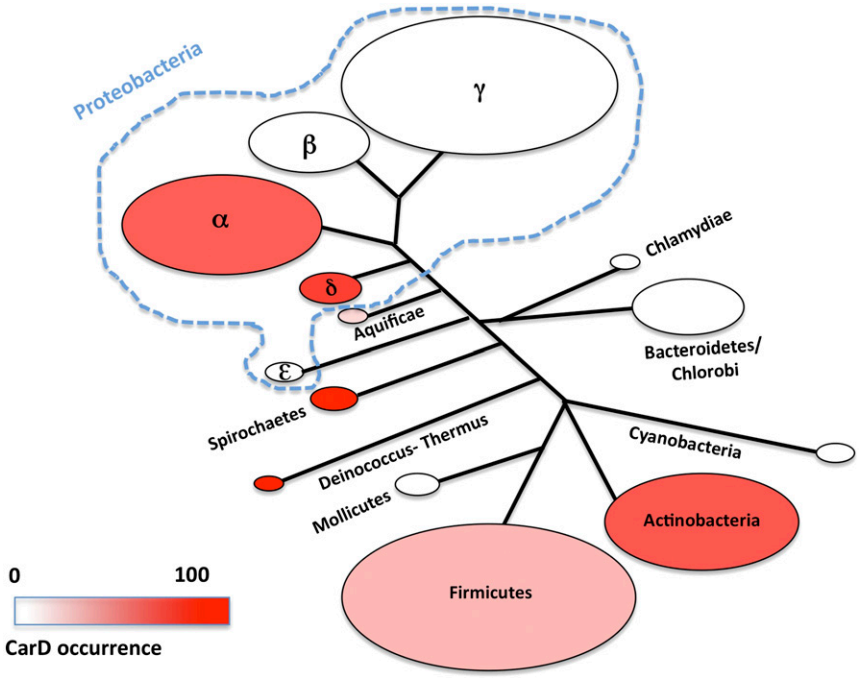

Fig. S1. Phylogenetic distribution of CarD. The BLAST database (www.ncbi.nlm.nih.gov/sutils/genom_table.cgi) containing completed genomes from 1,140 bacterial species (not including strains to avoid repeats and overrepresentation) was searched for *T. thermophilus* CarD homologs and returned 452 CarD homologs. The 1,140 species were schematically drawn on a phylogenetic tree, using a previously calculated phylogenetic distribution of bacteria based on the sequence conservation of the large RNAP subunits, β and β′ (1). The size of each oval represents the number of species sequenced in that particular group. The frequency of CarD found within each group was caclulated by counting the number of bacterial species encoding CarD and then plotted as a gradient within each group, using hues to represent the numerical frequency. Groups that have no color do not contain CarD.

1. Lane WJ, Darst SA (2010) Molecular evolution of multisubunit RNA polymerases: Sequence analysis. *J Mol Biol* 395(4):671–685.

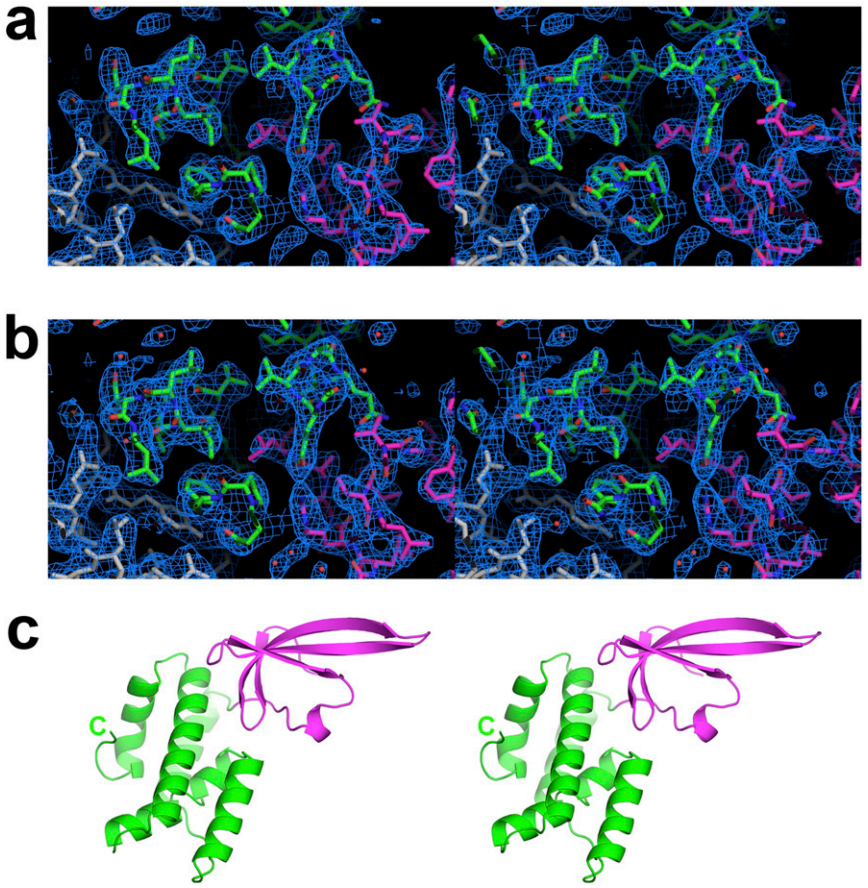

Fig. S2. Experimental electron density map of *T. thermophilus* CarD structure. (*A*) Stereoview of the unbiased experimental electron density map, contoured at 1σ. The final model is shown as sticks and colored according to Fig. 2*B*, with symmetry-related molecules colored gray. Nitrogen and oxygen atoms are colored blue and red, respectively. (*B*) Stereoview of 2fo-fc electron density map from the final refinement. Colors are as in *A*. (*C*) Stereoview of the *T. thermophilus* CarD structure, shown in ribbon format. Shown are same view and coloring as in Fig. 2*B*.

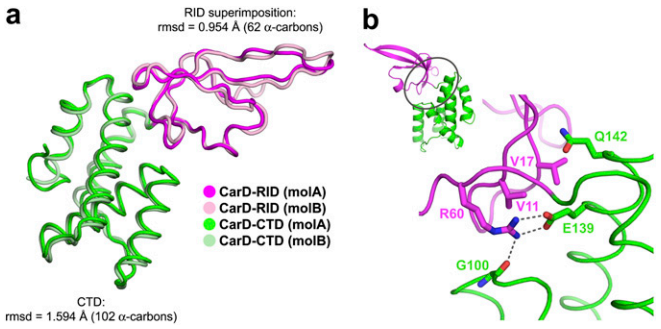

Fig. S3. Structural comparison of crystallographically independent *T. thermophilus* CarD molecules and interdomain interface. (*A*) The two crystallographically independent copies of *T. thermophilus* CarD (molA and molB) are shown in α-carbon backbone ribbon format. MolB is superimposed into molA by superimposition of 62 α-carbon positions in the N-terminal RID domain only (magenta), yielding an rmsd of 0.954 Å. The calculated rmsd for 102 α-carbon positions in the CTD (green) resulting from this superimposition was 1.594 Å, indicating that the orientations of the RID and CTD in the two molecules are nearly identical. (*B*) Conserved network of interactions at the CarD-RID/CarD-CTD interface. *Upper Left Inset* shows the ribbon diagram of *T. thermophilus* CarD (coloring as in *Lower Left*). The region enclosed in the gray ellipse is magnified in the *Lower Left*. In the magnified view, the α-carbon backbone is shown as a worm, and the side chains of residues involved in conserved interdomain interactions are shown.

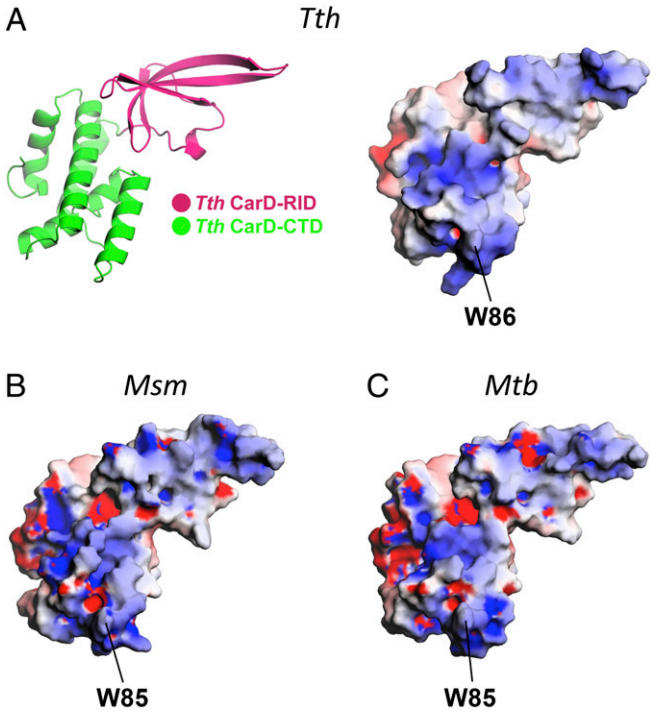

Fig. S4. Surface properties of *T. thermophilus* CarD are conserved in Mycobacterial CarD proteins. Analyses of the electrostatic surface distributions of *T. thermophilus*, *M. smegmatis*, and *M. tuberculosis* CarDs are shown. CarD-CTDs from all three organisms contain similarly positively charged faces on the CTD. (*A*) (*Left*) Ribbon rendering of *T. thermophilus* CarD shows the domain orientation. (*Right*) Molecular surface representation of *T. thermophilus* CarD (same orientation as the view at *Left*). Blue represents positively charged surfaces (+5 kT) and red negatively charged surfaces [−5 kT; calculated using APBS (1)]. (*B*) Molecular surface representation of a homology model of *M. smegmatis* CarD colored according to electrostatic surface distribution (+5 to −5 kT). (*C*) Molecular surface representation of a homology model of *M. tuberculosis* CarD colored according to electrostatic surface distribution (+5 to −5 kT). The homology models were calculated using the alignments shown in Fig. 2*A* with the program MODELER (2).

1. Baker NA, Sept D, Joseph S, Holst MJ, McCammon JA (2001) Electrostatics of nanosystems: Application to microtubules and the ribosome. *Proc Natl Acad Sci USA* 98(18):10037–10041.
2. Sali A, Potterton L, Yuan F, van Vlijmen H, Karplus M (1995) Evaluation of comparative protein modeling by MODELLER. *Proteins* 23(3):318–326.

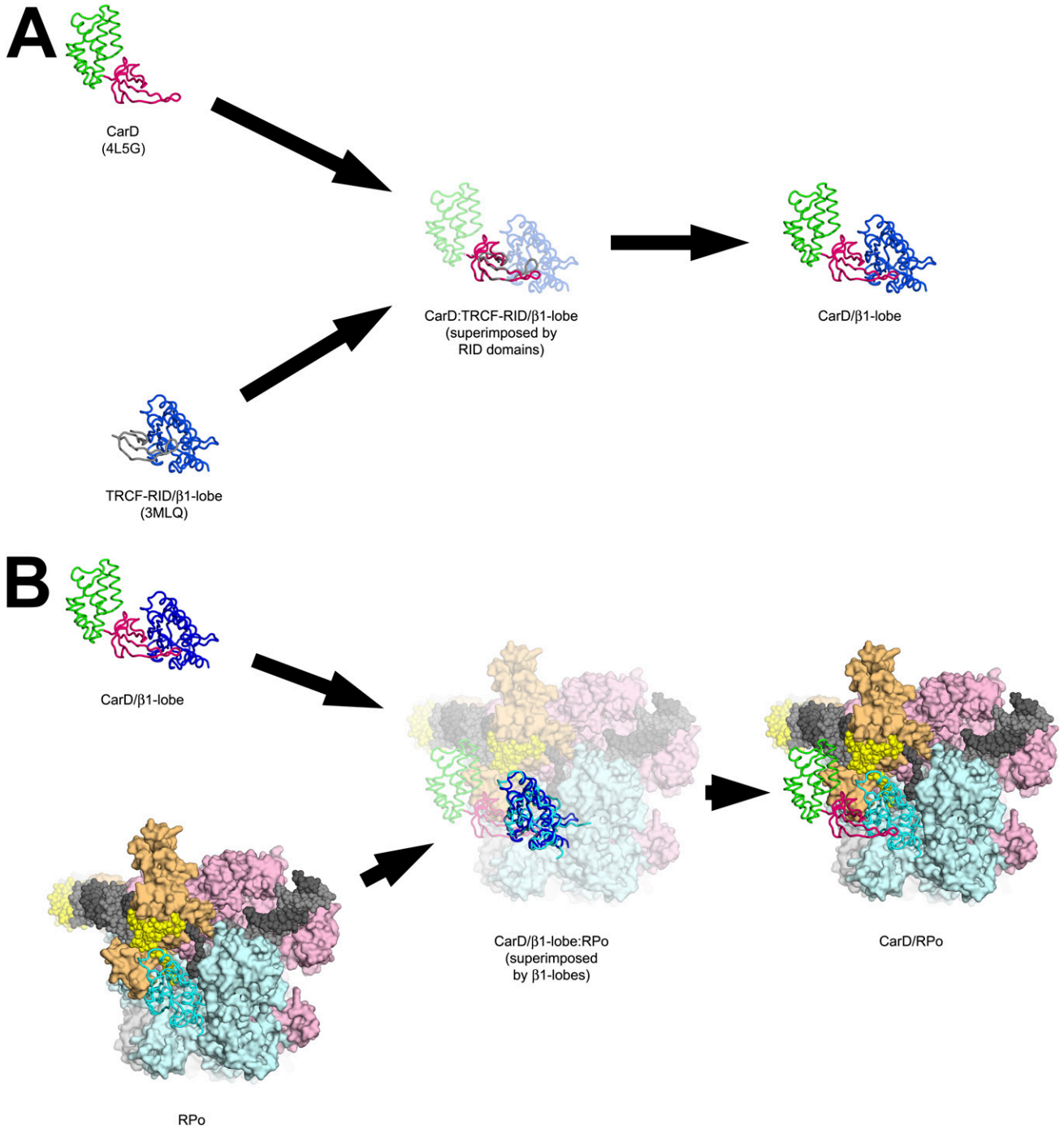

Fig. S5. Generation of *T. thermophilus* CarD/RNAP-holoenzyme open promoter (CarD/RPo) model. Diagram illustrates the steps used to generate the *T. thermophilus* CarD/RPo model (described in Fig. 3). (*A*) Generation of the *T. thermophilus* CarD/RNAP β1-lobe model. The RID domain of the *T. thermophilus* CarD X-ray crystal structure (reported herein, colored magenta, Fig. 2*B*) was superimposed onto the *T. thermophilus* transcription-repair coupling factor (TRCF)-RID (gray) from the TRCF-RID/β1-lobe X-ray crystal structure [Protein Data Bank (PDB) ID 3MLQ] (1). The two structural domains aligned with an rmsd of 1.061 Å over 27 α-carbon positions. (*B*) Generation of the *T. thermophilus* CarD/RPo model. The β1-lobe domain of the *T. thermophilus* CarD/β1-lobe model generated in *A* (blue) was superimposed onto the β1-lobe domain of a molecular model of the Taq RPo complex (2, 3). The two structural domains aligned with an rmsd of 1.8 Å over 154 α-carbon positions.

1. Westblade LF, et al. (2010) Structural basis for the bacterial transcription-repair coupling factor/RNA polymerase interaction. *Nucleic Acids Res* 38(22):8357–8369.
2. Feklistov A, Darst SA (2011) Structural basis for promoter-10 element recognition by the bacterial RNA polymerase σ subunit. *Cell* 147(6):1257–1269.
3. Murakami KS, Masuda S, Campbell EA, Muzzin O, Darst SA (2002) Structural basis of transcription initiation: An RNA polymerase holoenzyme-DNA complex. *Science* 296(5571): 1285–1290.

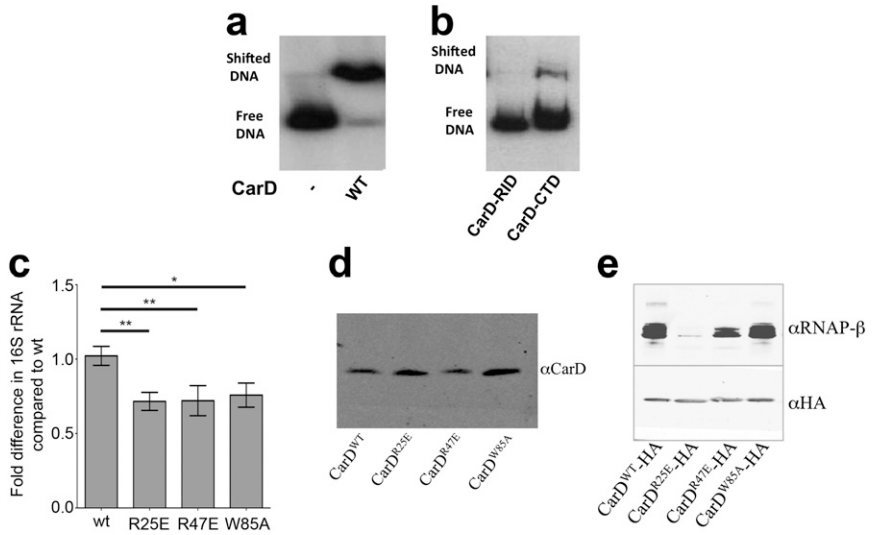

Fig. S6. CarD binds DNA without sequence specificity, the effects of CarD mutants on 16S rRNA levels in vivo, and mutant CarD binding to RNAP in vivo. (*A* and *B*) Autoradiographs of EMSAs with 200 pmol CarD, CarD domains (as labeled), or no protein (designated by –) incubated with 20,000 cpm (~0.6 ng) of [γ^{32}P]ATP-radiolabeled *rrnA*PL DNA. The reactions were separated on a nondenaturing polyacrylamide gel, which was then dried and exposed to film. (*C*) rRNA levels (16S) were measured by qRT-PCR, normalized to *sigA* transcript levels, and expressed as fold difference to CarD^{WT}-expressing cultures. The mean of four to five replicates is graphed and the error bars represent the SEM. Statistical significance of differences compared with CarD^{wt}-expressing strains were determined using *t* tests; $*P \leq 0.05$, $**P \leq 0.01$. (*D*) Fluorescent image of CarD protein levels in log-phase *M. smegmatis* Δ*carD attB*::*tet-carD* strains expressing CarD^{wt}, CarD^{R25E}, CarD^{R47E}, or CarD^{W85A}. These are the same strains used for qRT-PCR experiments in *C*. Total protein levels in the lysates were normalized before loading on the gel and CarD protein was detected by Western blotting with monoclonal antibodies specific for CarD. (*E*) Fluorescent image of CarD and RNAP β coimmunoprecipitated with a monoclonal antibody specific for HA in *M. smegmatis* strains expressing untagged CarD^{wt} (lane 1, also expresses HA peptide), CarD^{wt}-HA (lane 2), CarD^{R25E}-HA (lane 3), CarD^{R47E}-HA (lane 4), or CarD^{W85A}-HA (lane 5). Coprecipitated proteins in eluates were detected by Western blotting with antibodies specific for either RNAP β or CarD.

Table S1. ChIP-seq correlation coefficients

	HA	CarD-HA	RNAP β	σ^A
HA	0.934	0.530	0.730	0.417
CarD-HA		0.962	0.687	0.919
RNAP β			0.954	0.629
σ^A				1.000

The correlations table was obtained by computing the Pearson correlation of the genomic coverage profiles of each pair of samples. The coverage profiles were computed by summing the contributions of all mapped fragments, assuming they were 100 bp long, and then, in 20-bp steps along the entire genome, computing the average coverage of the surrounding 100-bp window. If a read mapped with equal quality at multiple loci (but not more than three), its contribution would be distributed among them (e.g., the reads that mapped to those two repetitive regions contributed 1/2 at each of the loci). If the number of mapping loci was higher than three, the read was discarded. Each sample was done in duplicate, except σ^A was done once. Correlations are the average of each duplicate to one another.

Table S2. Crystallographic statistics for *T. thermophilus* CarD crystals

Label	Native	Se1
Data collection		
Space group	$C222_1$	$C222_1$
Cell dimensions		
a, *b*, *c*, Å	74.795, 137.087, 103.450	75.128, 136.085, 104.896
α, β, γ, °	90, 90, 90	90, 90, 90
Wavelength	0.97920	0.97920
Resolution, Å	30.00–2.80 (2.90–2.80)	30.00–2.40 (2.49–2.40)
R_{sym} or R_{merge}	0.098 (0.983)	0.060 (0.560)
$I/\sigma I$	35.2 (2.6)	27.4 (2.3)
Completeness, %	100.0 (100.0)	99.9 (100.0)
Redundancy	11.9 (12.1)	4.2 (4.2)
Refinement		
Resolution, Å		30.00–2.40
No. reflections		40,928
R_{work}/R_{free}		0.2003/0.2297
No. atoms		
Protein		2,578
Ligand/ion		0
Water		96
B-factors		
Protein		61.33
Water		55.27
rms deviations		
Bond lengths, Å		0.005
Bond angles, °		0.872

Values in parentheses are for highest-resolution shell.